ACS APPLIED MATERIALS & INTERFACES

Research Article

www.acsami.org

Trap-Assisted Photomultiplication Polymer Photodetectors Obtaining an External Quantum Efficiency of 37 500%

Lingliang Li,[†] Fujun Zhang,*[,†] Wenbin Wang,[†] Qiaoshi An,[†] Jian Wang,[†] Qianqian Sun,[†] and Miao Zhang[†]

[†]Key Laboratory of Luminescence and Optical Information, Ministry of Education, Beijing Jiaotong University, Beijing 100044, People's Republic of China

Supporting Information

ABSTRACT: A smart strategy is reported to obtain photomultiplication (PM) type polymer photodetectors (PPDs) based on poly(3-hexylthiophene) (P3HT) and [6,6]-phenyl-C_{61}-butyric acid methyl ester ($PC_{61}BM$) which are commonly used in polymer solar cells. The PPDs with 1 wt % $PC_{61}BM$ exhibit a champion EQE of 37,500% under 625 nm illumination with an intensity of 8.87 μW cm^{-2} at −19 V bias. The PM phenomenon of PPDs with rather low $PC_{61}BM$ doping ratios should be attributed to the enhanced hole tunneling injection assisted by trapped electrons in $PC_{61}BM$ near the Al cathode, which can be completely demonstrated from (i) turning distribution of electron traps by changing P3HT:$PC_{61}BM$ doping weight ratios from 200:1 to 1:1; (ii) adjusting interfacial barrier width by inserting LiF layer between the active layer and the Al cathode.

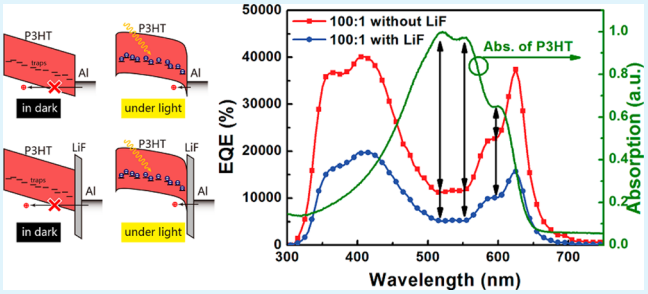

KEYWORDS: *organic photodetector, photomultiplication, trap, band bending, tunneling injection*

INTRODUCTION

Photodetectors based on organic semiconducting junctions have attracted more and more attention because of the attractive features of organic materials such as high extinction coefficient, adjustable band gap, and their potential applications in biomedical sensing, machine vision, and medical.[1,2] Most of the organic photodetectors are photodiodes with photoresponse that originates from the collection of photogenerated charge pairs. The external quantum efficiency (EQE) of photodiode type photodetectors is lower than 100% because of the limited photon harvesting efficiency, exciton dissociation efficiency, and photogenerated charge carrier collection efficiency. Photoelectron emission or avalanche effect cannot occur in organic semiconductors for obtaining highly sensitive photodetectors because of the relative large exciton binding energy of organic materials.[3,4] In recent years, highly sensitive organic or hybrid photodetectors have been successfully realized by using trap-assisted charge tunneling injection to achieve photomultiplication (PM) phenomenon, i.e., EQE in excess of 100%. The critical steps for obtaining PM phenomenon in organic or hybrid photodetectors are to realize large external charge injection under illumination and good transport in the active layer while keeping the opposite charges trapped in the active layer.[5] Yokoyama's group first reported a photomultiplication (PM) phenomenon in photodetectors based on organic pigment, with a peak internal quantum efficiency (IQE) of ∼10 000%.[6] Huang et al. reported C_{60}-based organic photodetectors with a maximum EQE of ∼8 000% due to interfacial trap-assisted charge carrier tunneling injection.[7] Wu et.al also reported PM type organic photodetectors with an EQE of ∼170%, based on interfacial traps in multiple layers.[8] Campbell et al. obtained an EQE of ∼10 000% by doping PbSe nanoparticles into poly[2-methoxy,5-(2′-ethylhexyloxy)-1, 4-phenylenevinylene] (MEH-PPV) polymer matrix, PbSe nanoparticles as electron traps, and MEH-PPV as hole transport channel.[9] Guo et al. reported PM-type photodetectors by interfacial trap-controlled charge injection based on ZnO nanoparticles doped into P3HT:$PC_{61}BM$ (1:1 weight ratio) system.[10] Recently, Park et al. reported a coplanar structure photoconductor based on blend film of poly dithienobenzodithiophene-*co*-diketopyrrolopyrrolebithiophene (PDPDBD) and $PC_{71}BM$ with weight ratio of 1:2 exhibiting an EQE of ∼1 × 10^7% under relatively high bias of about −190 V.[11] We summaried the major progresses in organic and hybrid photodetectors with trap-assisted PM phenomenon, as shown in Table 1. Up to now, PM-type polymer photodetectors (PPDs) with trap-assisted external charge injection have never been reported based on the ordinary P3HT:$PC_{61}BM$ system. Here, we report a new strategy to obtain PM-type PPDs based on the ordinary P3HT:$PC_{61}BM$ system, without any additional dopants or blocking layers, which is distinguished from the previous reports. This strategy may provide a new way for organic semiconducting materials to be used in high-performance photodetectors.

Received: January 5, 2015
Accepted: February 24, 2015
Published: February 26, 2015

DOI: 10.1021/acsami.5b00041
ACS Appl. Mater. Interfaces 2015, 7, 5890−5897

Table 1. Major Progresses in Organic and Hybrid Photodetectors with Trap-Assisted PM Phenomenon

year	λ (nm)	QE (%)	location of traps	materials and device structure	features	ref
1994	350−700	~10 000 (IQE)		Me-PTC/sandwich	the first reported PM type organic photodetectors	6
1999	450−520	~2000 (IQE)		arylamino-PPV/sandwich	PM type polymer photodetectors	12
2002	300−450	~20 000 (IQE)		NTCDA/sandwich	PM in organic single crystal	13
2007	350−700	~5000 (EQE)	bulk and interface	C_{60}/ sandwich	the first report that compares bulk traps with interfacial traps	7
2007	400−600	~10 000 (EQE)	doped bulk traps	MEH-PPV, PbSe, and $PC_{61}BM$/sandwich	PbSe quantum dots as traps in polymer matrix	9
2008	350−750	~8000 (EQE)	doped bulk traps	P3HT, $PC_{61}BM$ and CdTe/sandwich	CdTe nanoparticles as traps in ternary blend film	14
2010	300−1000	~7 000 (EQE)	doped bulk traps	P3HT, $PC_{61}BM$ and Ir125/sandwich	dye as traps in ternary blend film; extended spectral response to NIR	15
2010	350−600	~8 200 (EQE)	between molecular crystallites	Rubrene and DPA/coplanar	deep traps between molecular crystallites	16
2010	400−800	~34 000 (EQE) ~50 000 (IQE)	blocking layer	NTCDA/C_{60} as the hole blocking layers; CuPc/C_{60} as the active layers/sandwich	the first PM type organic photodetector based on charge blocking layer	17
2011	325	~1×10^5 (IQE)	additional trap layer	Grapheme,P3HT and $PC_{61}BM$/coplanar	P3HT or P3HT:$PC_{61}BM$ as electron trapping layer; graphene as hole transporting layer	18
2012	300−600	~3.4×10^5 (EQE)	doped bulk traps	P3HT, PVK and ZnO/sandwich	highest EQE among reported solid state UV-photodetectors	10
2012	400−1200	~5500 (EQE)	doped bulk traps	Ir125, Q-switch1, P3HT and $PC_{61}BM$	dual near-infrared dopants	19
2014	300−500	~400 (EQE)	interface	C-TPD, ZnO and C_{60}/ sandwich	linear dynamic range up to 120 dB	20
2014	350−1000	1624 (EQE)	doped bulk traps	PbS,P3HT,$PC_{61}BM$ and ZnO/sandwich	dual quantum dots and UV to NIR spectral response	21
2014	400−650	~1500 (EQE)	blocking layer	P3HT,$PC_{61}BM$/sandwich	semicontinuous blocking layer	5
2014	760	~1×10^7 (EQE)		PDPDBD,$PC_{71}BM$/coplanar	highest EQE among reported photoconductors	11

EXPERIMENTAL SECTION

Indium tin oxides (ITO) substrates with a sheet resistance of 15 Ω square^{-1} (purchased from Shenzhen Jinghua Display Co., Ltd.) were precleaned by ultrasonic treatment in detergent, deionized water, and ethanol in ultrasonic sequentially. Then, all ITO substrates were dried by nitrogen-gas and treated by UV-ozone for 10 min to further clean the ITO surface. The solution of PEDOT:PSS (Clevios P VP. Al 4083, purchased from Heraeus Precious Metal Gmbh & Co. KG) was spin-coated onto the ITO substrates at 5000 rounds per minute (rpm) for 40 s. The PEDOT:PSS-coated ITO substrates were baked in air at 120 °C for 10 min and then transferred to a nitrogen-filled glovebox (O_2 and H_2O concentrations <1 ppm). Poly(3-hexylthiophene) (P3HT) (Product No: LT-S909, purchased from Luminescence Technology Corp.) and [6,6]-phenyl-C_{61}-butyric acid methyl ester ($PC_{61}BM$) (Product No: PCBM-1−000000−14FM, purchased from FEM Technology Inc.) were dissolved in 1,2-dichlorobenzene (extra pure, purchased from J&K Scientific Ltd.) to prepare 40 mg mL^{-1} solutions, respectively. Then, the blend P3HT and $PC_{61}BM$ solutions were prepared with P3HT and $PC_{61}BM$ weight ratio from 200:1, 100:1, 100:15, to 1:1, respectively. The blend solutions of P3HT:$PC_{61}BM$ were spin-coated onto the PEDOT:PSS-coated ITO substrates at 800 rpm for 30 s to prepare the active layers. The 0.8 nm thickness LiF interfacial layer and 100 nm thickness aluminum (Al) cathode layer was deposited in vacuum (1×10^{-4} pa), which was monitored by a quartz crystal microbalance. The active area of each device is about 3.8 mm^2, which is defined by the vertical overlap of the ITO anode and the Al cathode. Current density versus voltage (J−V) and EQE spectra curves of the devices were measured by a Keithley 2400 source meter. The monochromatic light used in all these measurements was provided by a 150 W xenon lamp coupled with a monochromator. The monochromatic light intensity and wavelength were monitored and calibrated by a Newport 818-UV power meter and an Acton SpectraPro 2150i CCD spectrometer. Absorption spectra of films were measured by a Shimadzu UV-3101 PC spectrophotometer.

RESULTS AND DISCUSSION

The dark current density versus voltage (J_d−V) curves of all PPDs with or without LiF layer were measured under reverse bias and are shown in Figure 1. It is apparent that the dark

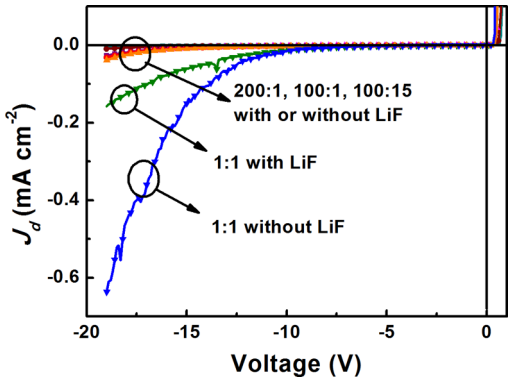

Figure 1. J_d−V curves of the PPDs with or without LiF interfacial layer.

current densities of PPDs with relatively low $PC_{61}BM$ doping ratios (≤15 wt %) are much lower than that of PPDs with P3HT:$PC_{61}BM$ (1:1) as the active layers under the same reverse bias, which can be well-explained by the energy levels of used materials, as shown in Figure S1b in the Supporting Information. Electrons can be easily injected from the Fermi level of ITO (−4.7 eV) onto the lowest unoccupied molecular orbital (LUMO) of $PC_{61}BM$ (−4.3 eV) because of the relatively small injection barrier of ~0.4 eV. Holes can be hardly injected from the Fermi level of Al (−4.2 eV) cathode onto the highest occupied molecular orbit (HOMO) of P3HT (−5.1 eV) because of the relatively larger hole injection barrier of ~0.9 eV. Therefore, the electron injection and transport in the $PC_{61}BM$ rich PPDs is much stronger than the other PPDs. It is known that the optimized doping ratio of P3HT:$PC_{61}BM$ is about 1:1 to form bicontinuous interpreting network for better charge-carrier transport in P3HT:$PC_{61}BM$-based polymer solar cells (PSCs).[22,23] Therefore, the electron transport ability of blend films can be markedly weakened along with the

DOI: 10.1021/acsami.5b00041
ACS Appl. Mater. Interfaces 2015, 7, 5890−5897

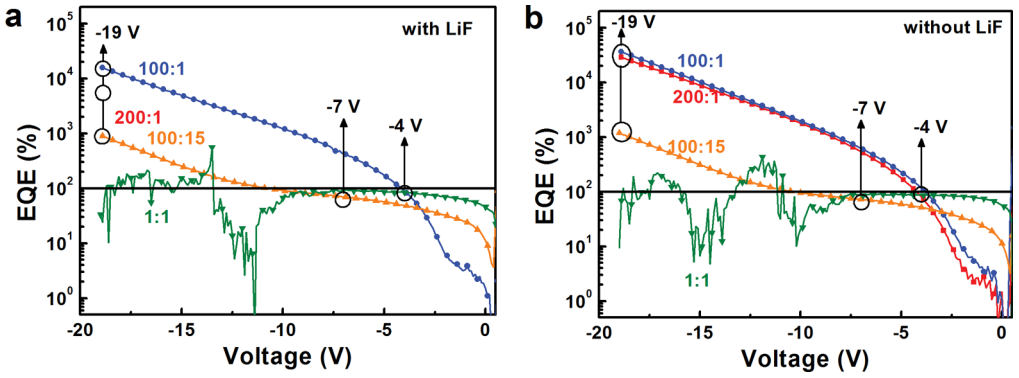

Figure 2. EQE−V curves of PPDs with different $PC_{61}BM$ doping ratios under 625 nm illumination with an intensity of 8.87 μW cm^{-2}: (a) with LiF layer, (b) without LiF layer.

Table 2. EQE Values of All PPDs at 625 nm Illumination with an Intensity of 8.87 μW cm^{-2}[a]

	−1 V		−2 V		−4 V		−7 V		−19 V	
LiF	W	W/O	W	W/O	W	W/O	W	W/O	W	W/O
1:1	61.9	75.9	70.4	82.5	84.5	86.8				
100:15	24.9	24.2	32.7	33.6	49.1	51.9	70.1	72.7	918	1190
100:1	3.34	4.26	6.14	8.41	89.9	116	430	626	16 300	37 500
200:1	1.96	2.48	2.98	3.68	22.9	80.4	167	544	5790	29 800

[a]W, with LiF layer; W/O, without LiF layer; blank entry, unstable.

decrease of $PC_{61}BM$ doping ratios. Meanwhile, hole transport ability of blend films should be increased because of the more ordered P3HT molecular arrangement for the fewer $PC_{61}BM$ dopant. The X-ray diffraction patterns of blend films with different $PC_{61}BM$ doping ratios were measured and are shown in Figure S2 in the Supporting Information. It is apparent that the diffraction intensity of the peak at $2\theta = 5.5°$ is increased along with the decrease of $PC_{61}BM$ doping ratios, which means that the P3HT molecular arrange become more and more ordered resulting in the increase of hole transport ability in the blend films.[24] Therefore, the blend films with low $PC_{61}BM$ doping ratios have great potential application in obtaining trap-assisted PM type PPDs according to the advantages: (i) hole can be transported faster than electron in the blend films; (ii) the dispersed $PC_{61}BM$ can be considered as electron traps according to the LUMOs offset 1.3 eV between $PC_{61}BM$ and P3HT, the trapped electrons in $PC_{61}BM$ may assist hole tunneling injection especially for those near the Al cathode. Hiramoto and Chen et al. reported that the trapped charges or the imbalanced transport of holes and electrons in the active layer can enable the distinct tunneling injection of external charges, which can realize the PM phenomenon in organic photodetectors.[6,25]

To confirm the effect of trap-assisted hole tunneling injection on the performance of PPDs, we measured the current density of all PPDs under 625 nm illumination with an intensity of 8.87 μW cm^{-2}. The EQE versus voltage (EQE−V) curves of all PPDs were calculated according to eq 1 and are shown in panels a and b in Figure 2, respectively.

$$\mathrm{EQE} = J_{ph}h\nu/I_{in}e = (J_l - J_d)h\nu/I_{in}e \quad (1)$$

where J_{ph} is photocurrent density, J_l is current density under light, J_d is dark current density, I_{in} is the incident light intensity, e is absolute value of electron charge, and $h\nu$ is the energy of incident photon. The detailed J_{ph}−V, J_l−V, and J_d−V curves of all the PPDs are shown in Figure S3 in the Supporting Information.

It is apparent that the EQE values of PPDs with P3HT:$PC_{61}BM$ (1:1) as the active layers rapidly arrive to about 86% (saturation states) along with reverse bias up to −4 V for the typical photovoltaic process, which means that photogenerated charge carriers can be effectively collected under the applied −4 V bias. Meanwhile, the PPDs with P3HT:$PC_{61}BM$ (1:1) as the active layers show an unstable characteristic due to the relatively large electron injected current under high reverse bias, which is also observed from the dark current curves, as shown in Figure 1. The electron transport channels formed by $PC_{61}BM$ would be damaged by overwhelming transporting electrons injected from the ITO anode, resulting in the unstable performance of PPDs under high reverse bias. However, the enhanced electron injected current has no contribution to J_{ph} and EQE values of PPDs, which can be demonstrated from the detailed J_{ph}−V, J_l−V, and J_d−V curves, as shown in Figure S3 in the Supporting Information. All the characteristics of the PPDs with P3HT:$PC_{61}BM$ (1:1) as active layer well accord with the previously reported photodiode type organic photodetectors.[26,27] In the following section, all the characterizations on photodiode type PPDs with P3HT:$PC_{61}BM$ (1:1) as active layer were carried out under low applied bias (−4 V) to give credible and repeatable experimental results.

An interesting phenomenon, EQE in excess of 100%, is observed from the PPDs with relatively low $PC_{61}BM$ doping weight ratios, as shown in Figure 2a, b. The detailed EQE values of all the PPDs are summarized under different reverse biases, as listed in Table 2. The EQE values of PPDs with 1 wt % $PC_{61}BM$ in the active layer arrive to about 16 300% and 37 500% at −19 V for the devices with or without LiF layer under 625 nm illumination with an intensity of 8.87 μW cm^{-2}, respectively. The PPDs with low $PC_{61}BM$ doping ratios can exhibit the rather high EQE values, which should be attributed

DOI: 10.1021/acsami.5b00041
ACS Appl. Mater. Interfaces 2015, 7, 5890−5897

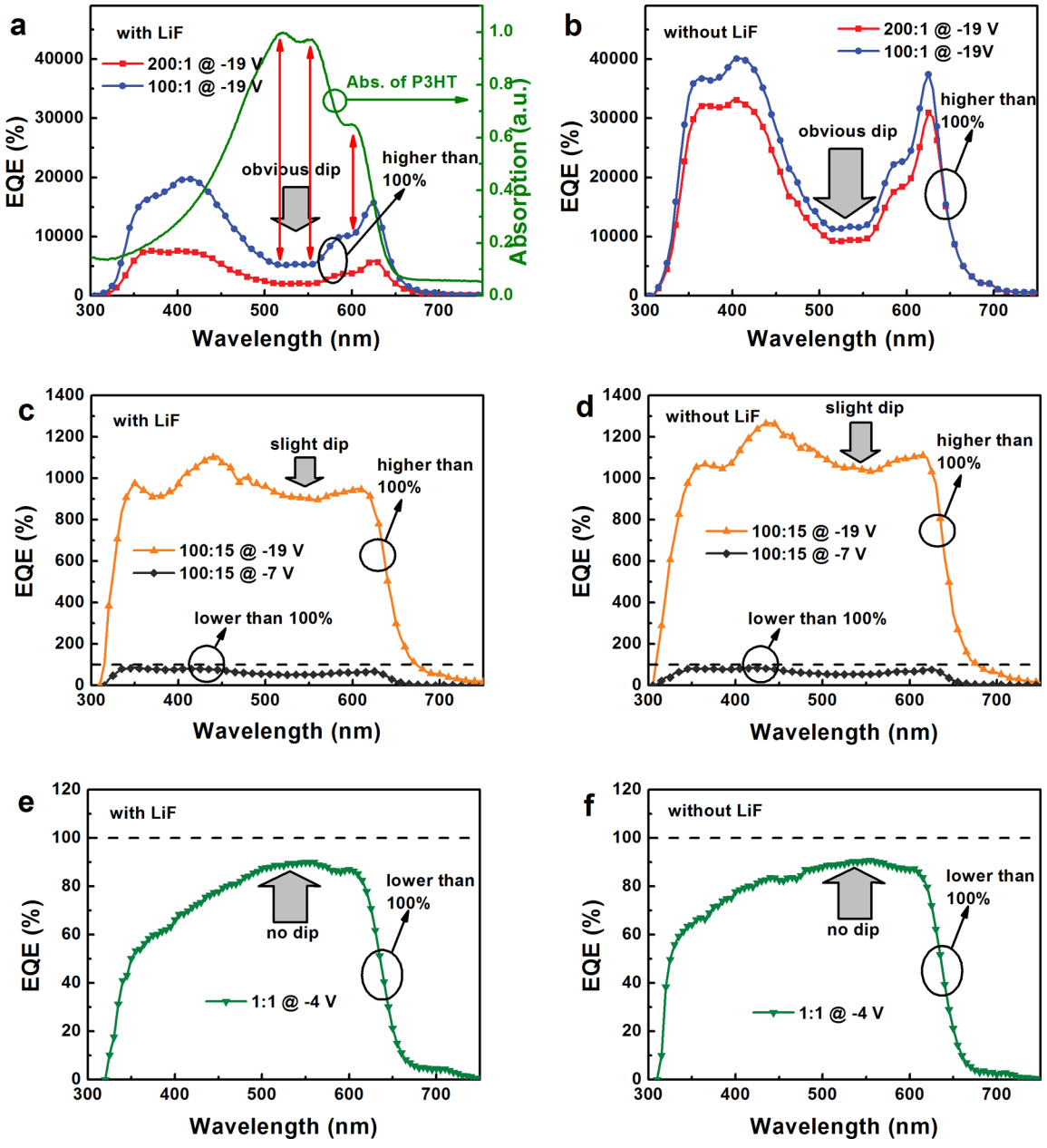

Figure 3. EQE spectra of all PPDs with different $PC_{61}BM$ doping ratios: (a, c, e) for the PPDs with LiF layer and (b, d, f) for the PPDs without LiF layer.

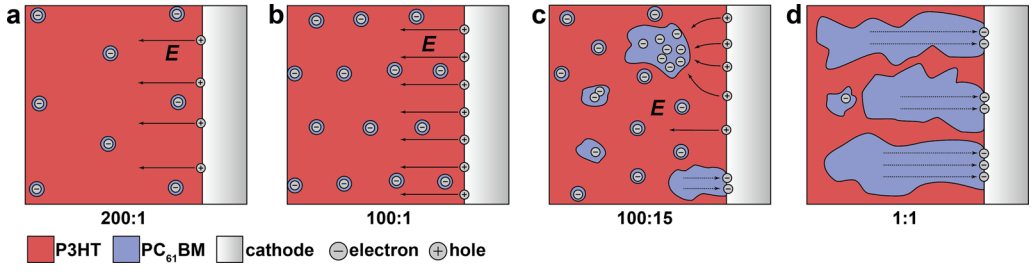

Figure 4. Behavior of electrons in PPDs with different P3HT:$PC_{61}BM$ doping ratios: (a) 200:1, (b) 100:1, (c) 100:15, (d) 1:1 for P3HT:$PC_{61}BM$ doping ratios.

to the trap assisted hole tunneling injection from the Al cathode into active layer. For PPDs with or without LiF layer, the PPDs with 1 wt % $PC_{61}BM$ exhibit the maximum EQE values. When $PC_{61}BM$ doping ratios are decreased from 1 wt % to 0.5 wt %, the EQE values are decreased from 16 300% to 5790% for PPDs with LiF layer, and are decreased 37 500% to 29 800% for PPDs without LiF layer. It means that the electron traps are mainly induced by doping $PC_{61}BM$ rather than intrinsic defect

DOI: 10.1021/acsami.5b00041
ACS Appl. Mater. Interfaces 2015, 7, 5890−5897

Table 3. Key Reverse Biases (voltage corresponding to EQE = 100%) of PM-Type PPDs

	100:15	100:1	200:1
with LiF	−10.8 V	−4.2 V	−6.0 V
without LiF	−10.3 V	−3.9 V	−4.3 V

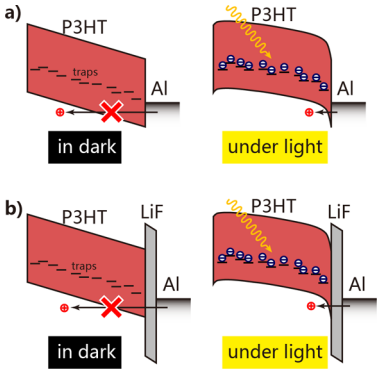

Figure 5. Schematic images of interfacial barriers of PM type PPDs under reverse bias in dark and under illumination (a) without LiF interfacial layer and (b) with LiF interfacial layer.

in P3HT films. It is worth mentioning that the PPDs with low $PC_{61}BM$ doping ratios have lower EQE values compared to PPDs with P3HT:$PC_{61}BM$ (1:1) as the active layers when the applied bias is lower than about −4 V. It should be attributed to the inefficient exciton dissociation and electron transport because of the relatively low $PC_{61}BM$ content in the blend films.

For the PPDs with 15 wt % $PC_{61}BM$, the champion EQE values arrive to about 910% or 1190% at −19 V bias for the devices with or without LiF layer, respectively. It should be highlighted that the EQE values of PPDs with 15 wt % $PC_{61}BM$ are much lower than those of PPDs with 1 or 0.5 wt % $PC_{61}BM$ under high reverse bias, which also further illustrates the key role of $PC_{61}BM$ disperse degree on the performance of PPDs. Meanwhile, the EQE values are lower than 100% while showing a saturation trend from 0 to −10 V, as shown in Figure 2a, b. It means that the PPDs with 15 wt % $PC_{61}BM$ exhibit photodiode characteristics under low reverse bias and PM characteristics under high reverse bias.

For PPDs with P3HT:$PC_{61}BM$ (1:1) as active layer, the EQE values of PPDs with or without LiF layer are increased from 61.9 to 84.5% or from 75.9 to 86.8% along the increase of bias from −1 to −4 V, respectively. And then the EQE values of this kind of PPDs come into saturation for the further increase of reverse bias, which means that the PPDs with P3HT:$PC_{61}BM$ (1:1) as active layer are photodiode type photodetectors. In the low reverse bias (<4 V) range, the enhanced EQE values should be attributed to effective charge carrier transport and collection along with the increase of applied bias.

To further clarify the key role of $PC_{61}BM$ doping ratios (dispersed degree) in the blend films on the EQE values of PPDs, we show the EQE spectra of all PPDs with different $PC_{61}BM$ doping ratios in Figure 3. An obvious dip can be observed from the EQE spectra of PPDs with P3HT:$PC_{61}BM$

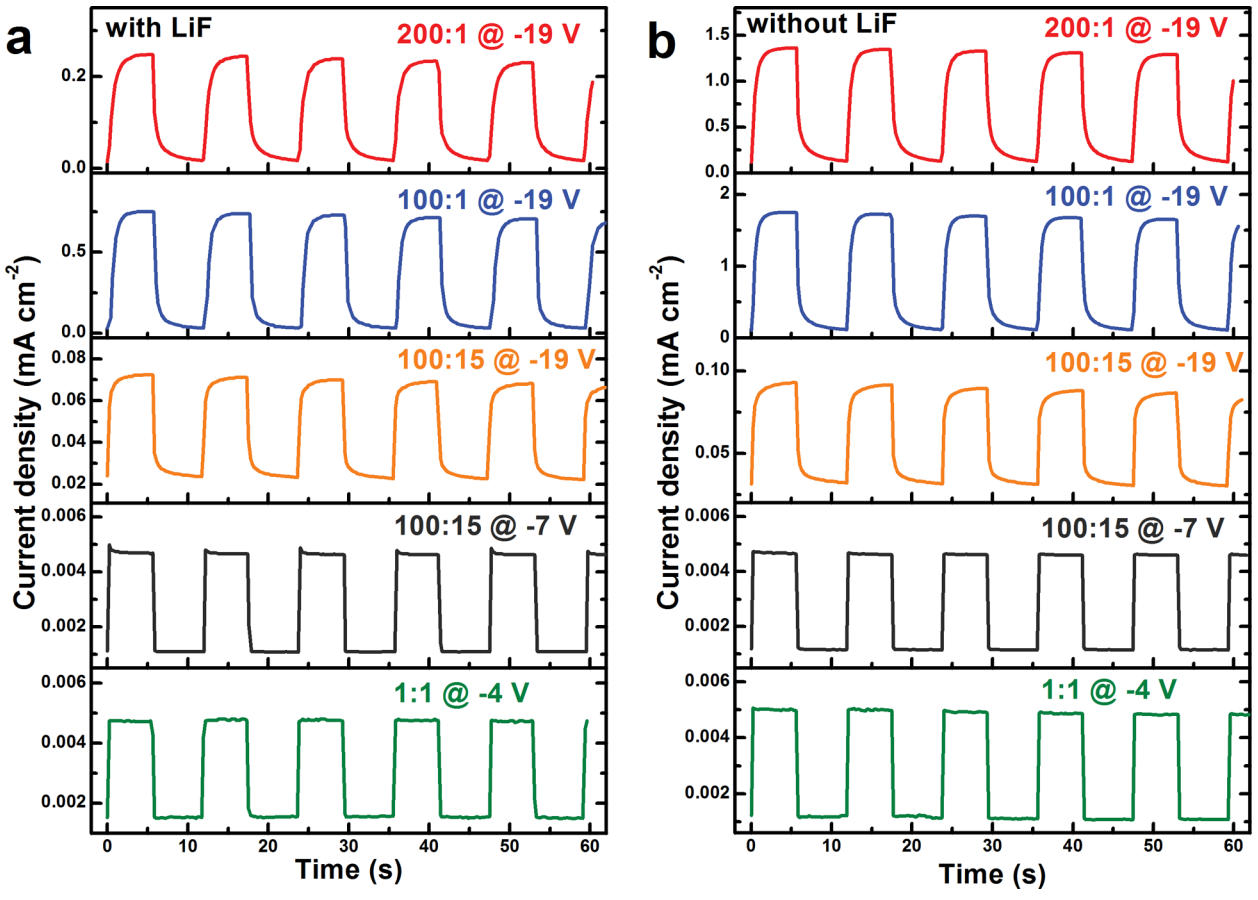

Figure 6. Transient current density of PPDs with different $PC_{61}BM$ doping ratios, (a) PPDs with LiF layer and (b) PPDs without LiF layer.

DOI: 10.1021/acsami.5b00041
ACS Appl. Mater. Interfaces 2015, 7, 5890−5897

(200:1 or 100:1 doping ratios) as active layer, as shown in Figure 3a, b. The dip in the EQE spectra exactly corresponds to the strong absorption range of neat P3HT films, the fine features between EQE spectra and absorption spectrum of P3HT are marked in Figure 3a. As we know, the incident photons from the ITO anode side will be rapidly absorbed by the active layer (mainly by P3HT) along with the propagation of incident light, excitons generated on P3HT near the Al anode are much fewer than those generated on P3HT near the ITO cathode. According to the previous works, only the charges trapped near the injecting interface can result in the interfacial band bending, which will contribute to the opposite charge tunneling injection.[21] The number of trapped electrons in $PC_{61}BM$ near the Al cathode is limited because of fewer photogenerated excitons in this spectral range, resulting in the weakened trap-assisted hole tunneling injection. This is the underlying reason for the obvious dip in the EQE spectra corresponding to the strong absorption range of P3HT.

As seen from the EQE spectra of PPDs with 15 wt % $PC_{61}BM$ in Figure 3c, d, EQE values are larger than 100% accompanying with a slight dip under −19 V bias. The champion EQE values of the PPDs with or without LiF layer arrive to about 1100% or 1300% under 445 nm illumination and −19 V bias, respectively. The PM phenomenon of these PPDs should be attributed to trap-assisted hole tunneling injection. The EQE values of the PPDs are lower than 100% under −7 V bias, as shown in the EQE spectra, which well accords with the experimental results shown in the EQE-*V* curves. As we may envisage, small molecule $PC_{61}BM$ would like aggregating to form some isolated clusters or even continuous electron transport channels in polymer matrix along with the increase of $PC_{61}BM$ doping ratios. Some large size isolated $PC_{61}BM$ clusters may be formed in the blend films with 15 wt % $PC_{61}BM$. We speculate that the trapped electrons in large size $PC_{61}BM$ clusters may have a small distance movement from near the ITO side to near the Al side, while they are still in the trapped state. The slight dip in EQE spectra indicates that most of the excitons generated on P3HT in the blend films (even near the ITO cathode) have contribution to the PM phenomenon, which strongly supports our speculation of the small distance movement of trapped electrons in large size $PC_{61}BM$ clusters. Therefore, it is apparent that relatively large size $PC_{61}BM$ clusters are formed in the blend film with 15 wt % $PC_{61}BM$, compared with the blend films with 1 and 0.5 wt % $PC_{61}BM$. The larger $PC_{61}BM$ isolated clusters not only collect more electrons generated from P3HT exciton dissociation, but are also more likely to link with the Al cathode, leading to the collection of the electrons in these $PC_{61}BM$ clusters. Once electrons in $PC_{61}BM$ are collected by the Al electrode rather than trapped in isolated $PC_{61}BM$ clusters, the trap-assisted hole tunneling injection will not take into effect, which is also strongly supported by the relatively low EQE values compared with the PPDs with 1 and 0.5 wt % $PC_{61}BM$. The EQE spectra of PPDs with P3HT:$PC_{61}BM$ (1:1) as the active layer are shown in Figure 3e, f. No dip in the EQE spectra can be observed and the EQE values of PPDs arrive to about 86% under −4 V bias. The EQE spectral shape of this kind of PPDs at −4 V bias is very similar to that of PSCs with the same active layer at zero bias.[28] To give a more intuitive explanation, the schematic images of the effect of $PC_{61}BM$ distribution on charge carrier injection and transport are shown in Figure 4.

It is known that the distribution of $PC_{61}BM$ should be relatively uniform in the whole blend films for the films with rather low $PC_{61}BM$ doping ratios, as shown in Figure 4a, b. The larger $PC_{61}BM$ clusters or even continuous electron transport channels will be formed along with the increase of $PC_{61}BM$ doping ratios, resulting in the nonuniform distribution of $PC_{61}BM$ in the blend films, as shown in Figure 4c, d. The trapped electrons can provide a Coulomb field to induce interfacial band bending which can assist hole tunneling injection from the Al cathode, especially for the trapped electrons in $PC_{61}BM$ near the Al cathode. The large $PC_{61}BM$ cluster not only harvest more electrons generated from P3HT exciton dissociation, but also capture more injected holes from the Al cathode to recombine with trapped electrons, as shown in Figure 4c. The number of trapped electron in $PC_{61}BM$ cluster near the Al cathode will be decreased because of the recombination, resulting in the weakened hole tunneling injection. Electrons in the $PC_{61}BM$ clusters contacting with the Al cathode can be easily transported to the Al cathode, which cannot give any contribution to enhance hole tunneling injection, as shown in Figure 4d. Therefore, the EQE values come into saturation state about 86% under at −4 V bias.

To further clarify the effect of trapped electrons in $PC_{61}BM$ near the Al cathode on hole tunneling injection shown in Figurse 2 and 3, we should further discuss the effect of LiF interfacial layer on EQE values. For the PPDs with relatively low $PC_{61}BM$ doping ratios (lower than 15 wt %), the EQE values of PPDs without LiF layer are larger than those of PPDs with LiF layer under relatively high applied bias. Inorganic material LiF has been widely used as ultrathin interfacial layer to enhance electron tunneling injection or collection in organic light emitting diodes or PSCs.[29,30] For the PPDs in this study, hole tunneling injection from the Al cathode into active layer will be more difficult due to the increased barrier width for the PPDs with LiF layer. According to the EQE-*V* curves shown in Figure 2, the key reverse biases (corresponding to EQE = 100%) of PM type PPDs with LiF layers are larger than those of PPDs without LiF layer, respectively, as summarized and listed in Table 3. The increase of key reverse biases should be attributed to the widened interfacial barrier due to the existence of LiF interfacial layer.

The schematic images of interfacial barriers of PM type PPDs under reverse bias in dark and under illumination are shown in Figure 5. The relatively high barrier of ∼0.9 eV prevents hole injection from Al cathode onto the HOMO of P3HT in dark condition, resulting in the low dark current of PM type PPDs. The photogenerated electrons trapped in the $PC_{61}BM$ can built up a Coulomb field in illumination condition. The band bending effect induced by the Coulomb field can narrow the interfacial barrier for better hole tunneling injection from Al cathode onto the HOMO of P3HT. For PM type PPDs with the LiF interfacial layer, hole injection barrier is increased because of the existence of LiF interfacial layer, which decreases the hole tunneling probability and leads to relatively low photocurrent and EQE values.

To further confirm the effect of $PC_{61}BM$ doping ratios and LiF layer on the performance of PPDs, we measured transient current density of all PPDs under the given applied bias, as shown in Figure 6a and 6b. The 625 nm illumination with an intensity of 8.87 $\mu W\ cm^{-2}$ was modulated by an electronic shutter with a period of about 12 s. For all the PM-type PPDs, the transient current density curves show slow rise and fall processes as the excitation light is turned on and off, respectively. As the above discussion, the photocurrent of PM-type PPDs is mainly the current which originates from the

DOI: 10.1021/acsami.5b00041
ACS Appl. Mater. Interfaces 2015, 7, 5890−5897

hole tunneling injection assisted by the trapped electrons in $PC_{61}BM$ aggregations. The slow rise and fall processes of transient photocurrent should be attributed to the slow accumulation and release processes of trapped electrons in the $PC_{61}BM$ clusters, which well accords with the trap-assisted PM model. The transient photocurrent of PM type PPDs comes into saturation state after excitation light is turned on, which means that the electron trapping and releasing processes arrives to a dynamic balance keeping a stable hole tunneling injection. When the excitation light is turned off, the photocurrent falling down to the initial state means that most of the trapped electrons have been released from electron traps formed by $PC_{61}BM$ clusters especially for those near the Al cathode. For the PPDs with P3HT:$PC_{61}BM$ (1:1) as the active layer, the rapid rise and fall processes can be observed when the excitation light is turned on or off, which obeys the photovoltaic process.[31] The amplitudes of the transient current densities of PPDs without LiF layer are larger than those of PPDs with LiF layer, which accords with the photocurrent densities observed from the steady $J-V$ curves. The transient current density curves provide a more solid evidence for the trap-assisted PM model.

CONCLUSION

PM-type PPDs are realized on the basis of the commonly used materials P3HT and $PC_{61}BM$ in polymer solar cells. The PPDs with P3HT:$PC_{61}BM$ (100:1) as the active layers exhibit a champion EQE value of 37,500% under 625 nm illumination with an intensity of 8.87 μW cm^{-2} at −19 V bias, which is among the highest reported values for organic/polymer photodetectors. The underlying reason for the PM phenomenon is attributed to the enhanced hole tunneling injection assisted by trapped electrons in $PC_{61}BM$ cluster near the Al cathode. The key role of trapped electrons in $PC_{61}BM$ near the Al cathode in obtaining PM phenomenon is fully demonstrated from EQE spectra, EQE−V curves and transient current density curves of PPDs with or without LiF layer. This discovery may provide a new route in fabricating highly sensitive organic/polymer photodetectors preserving all advantages of organic semiconducting materials.

ASSOCIATED CONTENT

Supporting Information

Device structure of the PPDs with or without the LiF buffer layer; energy level schematic diagram of used materials for PPDs in dark condition; the XRD diagrams of P3HT:$PC_{61}BM$ blend films with different weight ratios; the measured J_l, J_d, and calculated J_{ph} of all the PPDs with different P3HT:$PC_{61}BM$ doping ratios, with or without LiF layer; the on−off ratios (J_l to J_d) for PPDs under 625 nm illumination with an intensity of 8.87 μW cm^{-2}. This material is available free of charge via the Internet at http://pubs.acs.org.

AUTHOR INFORMATION

Corresponding Author

*E-mail: fjzhang@bjtu.edu.cn. Tel: 0086-10-51684908.

Notes

The authors declare no competing financial interest.

ACKNOWLEDGMENTS

This work was supported by National Natural Science Foundation of China (61377029), Fundamental Research Funds for the Central Universities (2014JBZ017), and Beijing Natural Science Foundation (2122050).

REFERENCES

(1) Dong, H. L.; Zhu, H. F.; Meng, Q.; Gong, X.; Hu, W. P. Organic Photoresponse Materials and Devices. *Chem. Soc. Rev.* **2012**, *41*, 1754−1808.
(2) Jansen-van Vuuren, R. D.; Pivrikas, A.; Pandey, A. K.; Burn, P. L. Colour Selective Organic Photodetectors Utilizing Ketocyanine-Cored Dendrimers. *J. Mater. Chem. C* **2013**, *1*, 3532−3543.
(3) Reynaert, J.; Arkhipov, V. I.; Heremans, P.; Poortmans, J. Photomultiplication in Disordered Unipolar Organic Materials. *Adv. Funct. Mater.* **2006**, *16*, 784−790.
(4) Pettersson, L. A. A.; Roman, L. S.; Inganäs, O. Quantum Efficiency of Exciton-to-Charge Generation in Organic Photovoltaic Devices. *J. Appl. Phys.* **2001**, *89*, 5564−5569.
(5) Melancon, J. M.; Živanović, S. R. Broadband Gain in Poly(3-Hexylthiophene):Phenyl-C61-Butyric-Acid-Methyl-Ester Photodetectors Enabled by A Semicontinuous Gold Interlayer. *Appl. Phys. Lett.* **2014**, *105*, 163301.
(6) Hiramoto, M.; Imahigashi, T.; Yokoyama, M. Photocurrent Multiplication in Organic Pigment Films. *Appl. Phys. Lett.* **1994**, *64*, 187.
(7) Huang, J.; Yang, Y. Origin of Photomultiplication in C_{60} Based Devices. *Appl. Phys. Lett.* **2007**, *91*, 203505.
(8) Wu, S. H.; Li, W. L.; Chu, B.; Su, Z. S.; Zhang, F.; Lee, C. S. High Performance Small Molecule Photodetector with Broad Spectral Response Range from 200 to 900 nm. *Appl. Phys. Lett.* **2011**, *99*, 023305.
(9) Campbell, I. H.; Crone, B. K. Bulk Photoconductive Gain in Poly(phenylene vinylene) Based Diodes. *J. Appl. Phys.* **2007**, *101*, 024502.
(10) Guo, F. W.; Yang, B.; Yuan, Y. B.; Xiao, Z. G.; Dong, Q. F.; Bi, Y.; Huang, J. S. A Nanocomposite Ultraviolet Photodetector Based on Interfacial Trap-Controlled Charge Injection. *Nat. Nanotechnol.* **2012**, *7*, 798−802.
(11) Park, S.; Lim, B. T.; Kim, B.; Son, H. J.; Chung, D. S. High Mobility Polymer Based on A π-Extended Benzodithiophene and Its Application for Fast Switching Transistor and High Gain Photoconductor. *Sci. Rep.* **2014**, *4*, 5482.
(12) Däubler, T. K.; Neher, D.; Rost, H.; Hörhold, H. H. Efficient Bulk Photogeneration of Charge Carriers and Photoconductivity Gain in Arylamino-PPV Polymer Sandwich Cells. *Phys. Rev. B* **1999**, *59*, 1964−1972.
(13) Hiramoto, M.; Miki, A.; Yoshida, M.; Yokoyama, M. Photocurrent Multiplication in Organic Single Crystals. *Appl. Phys. Lett.* **2002**, *81*, 1500−1502.
(14) Chen, H. Y.; LoMichael, K. F.; Yang, G.; Monbouquette, H. G.; Yang, Y. Nanoparticle-assisted High Photoconductive Gain in Composites of Polymer and Fullerene. *Nat. Nanotechnol.* **2008**, *3*, 543−547.
(15) Chen, F. C.; Chien, S. C.; Cious, G. L. Highly Sensitive, Low-voltage, Organic Photomultiple Photodetectors Exhibiting Broadband Response. *Appl. Phys. Lett.* **2010**, *97*, 103301.
(16) Hernandez-Sosa, G.; Coates, N. E.; Valouch, S.; Moses, D. High Photoconductive Responsivity in Solution-Processed Polycrystalline Organic Composite Films. *Adv. Funct. Mater.* **2011**, *21*, 927−931.
(17) Hammond, W. T.; Xue, J. Organic Heterojunction Photodiodes Exhibiting Low Voltage, Imaging-Speed Photocurrent Gain. *Appl. Phys. Lett.* **2010**, *97*, 073302.
(18) Tan, W. C.; Shih, W. H.; Chen, Y. F. A Highly Sensitive Graphene-Organic Hybrid Photodetector with a Piezoelectric Substrate. *Adv. Funct. Mater.* **2014**, *24*, 6818−6825.
(19) Chuang, S. T.; Chien, S. C.; Chen, F. C. Extended Spectral Response in Organic Photomultiple Photodetectors Using Multiple Near-Infrared Dopants. *Appl. Phys. Lett.* **2012**, *100*, 013309.
(20) Fang, Y.; Guo, F.; Xiao, Z.; Huang, J. Large Gain, Low Noise Nanocomposite Ultraviolet Photodetectors with a Linear Dynamic Range of 120 dB. *Adv. Opt. Mater.* **2014**, *2*, 348−353.

DOI: 10.1021/acsami.5b00041
ACS Appl. Mater. Interfaces 2015, 7, 5890−5897

(21) Dong, R.; Bi, C.; Dong, Q.; Guo, F.; Yuan, Y.; Fang, Y.; Xiao, Z.; Huang, J. An Ultraviolet-to-NIR Broad Spectral Nanocomposite Photodetector with Gain. *Adv. Opt. Mater.* **2014**, *2*, 549−554.
(22) An, Q. S.; Zhang, F. J.; Li, L. L.; Wang, J.; Zhang, J.; Zhou, L. Y.; Tang, W. H. Improved Efficiency of Bulk Heterojunction Polymer Solar Cells by Doping Low-Bandgap Small Molecules. *ACS Appl. Mater. Interfaces* **2014**, *6*, 6537−6544.
(23) An, Q. S.; Zhang, F. J.; Li, L. L.; Zhuo, Z. L.; Zhang, J.; Tang, W. H.; Teng, F. Enhanced Performance of Polymer Solar Cells by Employing A Ternary Cascade Energy Structure. *Phys. Chem. Chem. Phys.* **2014**, *16*, 16103−16109.
(24) Kim, B. G.; Kim, M. S.; Kim, J. Ultrasonic-Assisted Nanodimensional Self-Assembly of Poly-3-hexylthiophene for Organic Photovoltaic Cells. *ACS Nano* **2010**, *4*, 2160−2166.
(25) Chen, H. Y.; Lo, M. K. F.; Yang, G. W.; Monbouquette, H. G.; Yang, Y. Nanoparticle-Assisted High Photoconductive Gain in Composites of Polymer and Fullerene. *Nat. Nanotechnol.* **2008**, *3*, 543−547.
(26) Pace, G.; Grimoldi, A.; Natali, D.; Sampietro, M.; Coughlin, J. E.; Bazan, G. C.; Caironi, M. All-Organic and Fully-Printed Semitransparent Photodetectors Based on Narrow Bandgap Conjugated Molecules. *Adv. Mater.* **2014**, *26*, 6773−6777.
(27) Yang, D. Z.; Xu, K.; Zhou, X. K.; Wang, Y. P.; Ma, D. G. Comprehensive Studies of Response Characteristics of Organic Photodetectors Based on Rubrene and C-60. *J. Appl. Phys.* **2014**, *115*, 244506.
(28) Zhang, F. J.; Zhuo, Z. L.; Zhang, J.; Wang, X.; Xu, X. W.; Wang, Z. X.; Xin, Y. S.; Wang, J.; Wang, J.; Tang, W. H.; Xu, Z.; Wang, Y. S. Influence of $PC_{60}BM$ or $PC_{70}BM$ as Electron Acceptor on The Performance of Polymer Solar Cells. *Sol. Energy Mater. Sol. Cells* **2012**, *97*, 71−77.
(29) Chen, L.; Jiang, Y. B.; Nie, H.; Hu, R. R.; Kwok, H. S.; Huang, F.; Qin, A. J.; Zhao, Z. J.; Tang, B. Z. Rational Design of Aggregation-Induced Emission Luminogen with Weak Electron Donor-Acceptor Interaction to Achieve Highly Efficient Undoped Bilayer OLEDs. *Acs Appl. Mater. Interfaces* **2014**, *6*, 17215−17225.
(30) Jeon, Y. J.; Yun, J. M.; Kim, D. Y.; Na, S. I.; Kim, S. S. Moderately Reduced Graphene Oxide as Hole Transport Layer in Polymer Solar Cells via Thermal Assisted Spray Process. *Appl. Surf. Sci.* **2014**, *296*, 140−146.
(31) Kang, T. E.; Cho, H. H.; Cho, C. H.; Kim, K. H.; Kang, H.; Lee, M.; Lee, S.; Kim, B.; Im, C.; Kim, B. J. Photoinduced Charge Transfer in Donor-Acceptor (DA) Copolymer: Fullerene Bis-adduct Polymer Solar Cells. *Acs. Appl. Mater. Interfaces* **2013**, *5*, 861−868.

DOI: 10.1021/acsami.5b00041
ACS Appl. Mater. Interfaces 2015, 7, 5890−5897